

StableQAT: Stable Quantization-Aware Training at Ultra-Low Bitwidths

Tianyi Chen ^{*1} Sihan Chen ^{*2} Xiaoyi Qu ^{*3} Dan Zhao ^{*4} Ruomei Yan ¹ Jongwoo Ko ¹ Luming Liang ¹
Pashmina Cameron ¹

Abstract

Quantization-aware training (QAT) is essential for deploying large models under strict memory and latency constraints, yet achieving stable and robust optimization at ultra-low bitwidths remains challenging. Common approaches based on the straight-through estimator (STE) or soft quantizers often suffer from gradient mismatch, instability, or high computational overhead. As such, we propose StableQAT, a unified and efficient QAT framework that stabilizes training in ultra low-bit settings via a novel, lightweight, and theoretically grounded surrogate for backpropagation derived from a discrete Fourier analysis of the rounding operator. StableQAT strictly generalizes STE as the latter arises as a special case of our more expressive surrogate family, yielding smooth, bounded, and inexpensive gradients that improve QAT training performance and stability across various hyperparameter choices. In experiments, StableQAT exhibits stable and efficient QAT at 2-4 bit regimes, demonstrating improved training stability, robustness, and superior performance with negligible training overhead against standard QAT techniques. Our code is available at <https://github.com/microsoft/StableQAT>.

1. Introduction

Large language models (LLMs) are increasingly deployed under strict constraints on memory bandwidth, energy consumption, and hardware throughput, making full-precision inference impractical at scale. Quantization of weights and activations has therefore become a key technique for efficient deployment. Although post-training quantization (PTQ) achieves competitive accuracy at 8-bit precision, its performance degrades sharply below 4 bits due to the het-

^{*}Equal contribution ¹Microsoft ²Renmin University of China
³Lehigh University ⁴New York University. Correspondence to: Tianyi Chen <Tianyi.Chen@microsoft.com>.

Preprint, copyright 2026, (*) core contributors.

erogeneous distributions (Ding et al., 2023), motivating the use of quantization-aware training (QAT) (Frantar et al., 2023; Xiao et al., 2023; Liu et al., 2024a). QAT addresses this limitation by exposing models to quantization effects during training, allowing models to adapt to noise from discretization (Jacob et al., 2018).

Quantization-aware training (QAT) exhibits increasing optimization fragility as target bitwidths decrease, with both stability and accuracy becoming difficult to maintain at and below 4-bit precision (Du et al., 2024b; Panferov et al., 2025). Recent studies attribute this instability to multiple interacting factors, including outlier-dominated distributions, sensitivity to quantizer scaling and clipping, complex optimizer-quantization interactions, and the accumulation of approximation errors across layers (Choi et al., 2018; Esser et al., 2019). Although many methods attempt to mitigate these issues from different perspectives (Kundu et al., 2024; Chen et al., 2025), low-bit QAT remains unstable and often yields suboptimal performance. A key underlying reason is that existing approaches are unable to effectively resolve the fundamental mismatch between the discrete quantization process in the forward pass and continuous gradient-based optimization in the backward pass.

Forward-Backward Mismatch in QAT. A central challenge in QAT arises from the rounding operator. Exact quantization relies on hard rounding to map continuous values to discrete levels, yet the rounding function is non-differentiable and has zero gradient almost everywhere. To enable backpropagation, the straight-through estimator (STE) is commonly adopted as a surrogate (Bengio et al., 2013b; Hubara et al., 2018). While STE makes QAT practically usable, it introduces a significant approximation error in the optimization direction, which often leads to unstable training, especially at low bitwidths. Recent approaches attempt to address this mismatch by introducing differentiable or stochastic relaxations of quantization, including noise-based training, soft rounding, and smooth approximations that gradually anneal toward discrete behavior (Gong et al., 2019; Zhong et al., 2023; Défossez et al., 2022; Huang et al., 2022; Semenov, 2025). Although these methods smoothen the optimization process, they typically incur additional computational overhead, introduce extra

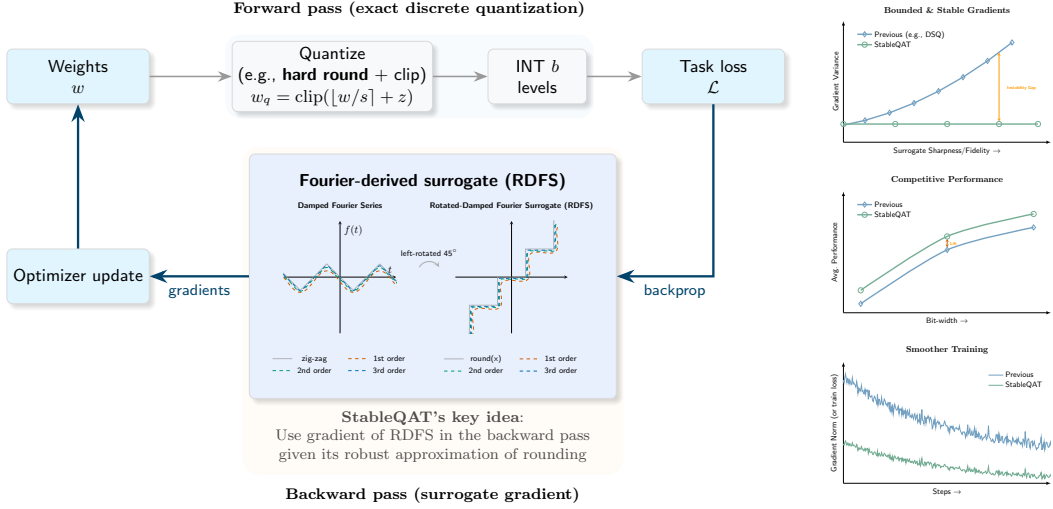


Figure 1. StableQAT procedure.

variance, or require careful scheduling to balance fidelity to discrete inference against optimization stability.

1.1. Contributions

We introduce **StableQAT**, a simple but flexible and effective framework to address the optimization bottlenecks of QAT that can be seamlessly integrated into existing training pipelines. StableQAT introduces a *rotated Fourier surrogate* that models the rounding operator through its spectral structure, yielding a smooth and bounded optimization direction. As a result, StableQAT provides a theoretically grounded and computationally efficient plug-and-play solution to stabilize and boost QAT performance. Our main contributions are summarized as follows.

- **Rotated Damped Fourier Surrogate (RDFS).** We propose a novel surrogate for the quantization operator by modeling quantization via a Fourier analysis, applying a geometric rotation, and damping the amplitude, yielding a computationally efficient, smooth, bounded, and stable optimization behavior for QAT.
- **Theoretical Analysis.** We provide comprehensive theoretical insights into the properties of our proposed rotated fourier surrogate, including its approximation error and variance, revealing its advantages compared to STE and prior soft rounding alternatives.
- **Robust Performance & Stability.** Extensive experiments demonstrate that StableQAT achieves consistently improved training stability and LLM performance at 2-4 bit precision, without incurring additional computational overhead compared to standard QAT.

Table 1. Qualitative comparison of QAT methods.

Characteristic	StableQAT	DSQ	ParetoQ
Theoretically grounded surrogate	✓	✓	✗
Computationally lightweight	✓	✗	✓
Bounded gradient variance	✓	✗	✗
Low-bit training & performance stability	✓	✗	✗

2. Preliminary and Related Work

This section reviews the necessary preliminaries and the most closely related works. Additional discussions on post-training quantization (PTQ) and other quantization-aware training (QAT) paradigms are deferred to Appendix A.

2.1. Quantization

Quantization maps high-precision floating values (e.g., FP32 or FP16) into low-precision discrete representations (e.g., INT8 or INT4), thereby reducing memory footprint and inference-time computational cost. Given a floating-point variable x_{original} (e.g., weights or activations) and a target bit-width b , a quantizer maps x_{original} to an integer domain $[q_{\min}, q_{\max}]$. For signed quantization, the range is typically $[-2^{b-1}, 2^{b-1} - 1]$, and becomes $[0, 2^b - 1]$ for unsigned quantization.

The quantization process is parameterized by a scaling factor $s \in \mathbb{R}^+$ and a zero-point $z \in \mathbb{Z}$, and is defined as:

$$x_q = \text{clip} \left(\text{round} \left(x_{\text{original}} / s \right) + z, q_{\min}, q_{\max} \right) \quad (1)$$

$$= \text{clip} \left(\text{round} \left(x \right) + z, q_{\min}, q_{\max} \right),$$

where $\text{round}(\cdot)$ denotes the round-to-nearest-integer oper-

ator, and $\text{clip}(v, a, b) = \min(\max(v, a), b)$ enforces the feasible range constraint. We denote $x \triangleq x_{\text{original}}/s$ for simplicity of notations. Here, the scaling factor s (also referred to as the quantization step size) determines the quantization resolution, while the zero-point z controls the alignment between the floating-point and integer domains. Without loss of generality, we assume $z = 0$ throughout the remainder of this paper for notational simplicity. We note that our analysis remains valid for arbitrary z .

2.2. Straight-Through Estimator (STE)

Training quantized networks poses a fundamental optimization challenge due to the non-differentiability of the rounding operation in Eq. (1). In particular, the rounding function has zero derivative almost everywhere and is undefined at integer transition points. As a result, its first-order derivative carries no informative signal, causing standard backpropagation to fail with ineffective parameter updates under gradient-based optimization.

To address this, the Straight-Through-Estimator (STE) (Bengio et al., 2013a) has been widely adopted to provide a surrogate to the derivative. STE simply ignores the rounding operation during the backward pass and approximates the differential of the quantized value x_q with respect to the input x as an identity function. More formally, let \mathcal{L} denote the task loss. The derivative of the loss with respect to the pre-quantized input x is then approximated by STE as:

$$\frac{\partial \mathcal{L}}{\partial x} = \frac{\partial \mathcal{L}}{\partial x_q} \cdot \left[\frac{\partial x_q}{\partial x} \right]_{\text{STE}} \approx \frac{\partial \mathcal{L}}{\partial x_q}, \quad (2)$$

where the true derivative $\partial x_q / \partial x$ is replaced by an identity surrogate. Although STE makes QAT practically feasible, it introduces substantial gradient mismatch due to the large deviation between the straight-through surrogate and the rounding operator. This mismatch injects significant optimization noise, leading to biased and unstable gradient updates, impaired convergence behavior, and ultimately sub-optimal performance, especially at ultra-low bitwidths.

2.3. Soft Surrogate Quantization

Soft surrogate quantization methods more directly target the rounding operation by introducing continuous relaxations. DSQ (Gong et al., 2019) is a representative approach that employs a parameterized \tanh function whose sharpness is gradually increased during training. More recent work (Semenov, 2025) utilizes a sigmoid function to smooth the rounding operator in Equation 1.

While these approaches capture richer structural information of the quantization process, they still suffer from the inherently ill-conditioned optimization landscape induced by the rounding operator. Moreover, they rely on com-

putationally expensive \exp -based functions, significantly slowing down training, typically by $3\times$ – $5\times$ in both forward and backward passes (see Figure 5). Other soft quantization methods introduce additional relaxation regularizers; however, they continue to face similar optimization challenges stemming from the underlying rounding behavior.

3. StableQAT

StableQAT is a simple QAT framework that addresses the critical forward-backward mismatch challenges of low-bit optimization. StableQAT achieves improved training stability and higher performance without incurring additional computational cost. At its core, StableQAT is built upon a **Rotated Damped Fourier Surrogate (RDFS) of the quantization operator**. The key idea is to model the discrete quantization process via a Fourier series and to derive a smooth, analytically grounded surrogate for backpropagation through a geometric rotation of this representation. This construction yields a stable and well-behaved optimization direction for gradient-based training.

Backward Pass via RDFS: As illustrated in Figure 2, we approximate the rounding operator using a Rotated Damped Fourier Surrogate (RDFS). By preserving richer structural information of the rounding operation, RDFS provides more informative learning signals while addressing the ill-defined Jacobian $\partial x_q / \partial x$, thereby stabilizing and improving gradient-based QAT. Formally, the derivative with respect to the input x is computed by RDFS as:

$$\frac{\partial \mathcal{L}}{\partial x} = \frac{\partial \mathcal{L}}{\partial x_q} \cdot \left[\frac{\partial x_q}{\partial x} \right]_{\text{RDFS}} \approx \frac{\partial \mathcal{L}}{\partial x_q} \cdot g(x, x_q), \quad (3)$$

where our proposed rotated Fourier surrogate $g(x, x_q)$ is defined as:

$$g(x, x_q) = \frac{1 - A\sqrt{2}\pi \sum_{m=0}^M \frac{(-1)^m}{2m+1} \cos((2m+1)\pi(x + x_q))}{1 + A\sqrt{2}\pi \sum_{m=0}^M \frac{(-1)^m}{2m+1} \cos((2m+1)\pi(x + x_q))}. \quad (4)$$

In practice, we truncate the series and typically use the first-order RDFS (i.e., $M = 0$):

$$g(x, x_q) = \frac{1 - A\sqrt{2}\pi \cos(\pi(x + x_q))}{1 + A\sqrt{2}\pi \cos(\pi(x + x_q))}. \quad (5)$$

Here, A is a tunable hyperparameter controlling the sharpness of the surrogate. The derivation, based on a geometric rotation and Fourier analysis, is provided in the following.

STE as a Special Case of RDFS. Note that $A = 0$, the RDFS degenerates to identity mapping, which exactly becomes the Straight-Through Estimator (STE). It shows that STE is a special case of RDFS, and highlights the increased

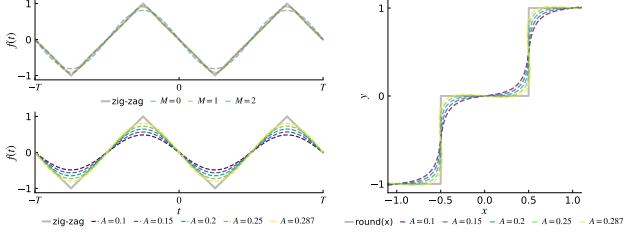


Figure 2. Rotated Damped Fourier Surrogate (RDFS) under different orders and amplitudes.

generality of RDFS, revealing that the potential of RDFS to **carry-out richer structural information leading towards stronger convergence and better performance**.

3.1. Rotated Damped Fourier Surrogate (RDFS)

Coordinate Rotation. We observe that applying a 45° counterclockwise rotation to the coordinate system (x, x_q) transforms the staircase-shaped rounding operator into a periodic, continuous, piecewise-linear function, commonly referred to as a triangle wave function, shown in Figure 2.

More formally, we introduce a rotated coordinate system $(t, f(t))$ obtained by rotating the original coordinates (x, x_q) by an angle $\theta = 45^\circ$ counterclockwise. The resulting coordinates are given by

$$t = \frac{x + x_q}{\sqrt{2}}, \quad f(t) = \frac{-x + x_q}{\sqrt{2}}. \quad (6)$$

Under the rotated coordinate system, the rounding operator becomes a periodic zig-zag function with fundamental period $T = \sqrt{2}$. Specifically, the transformed function can be expressed as a centered triangle wave:

$$f(t) = \frac{1}{2\sqrt{2}} \left(1 - 4 \left| r(t) - \frac{1}{2} \right| \right), \quad (7)$$

where $r(t) = \left\{ \frac{t-T/4}{T} \right\}$ denotes the phase-shifted fractional part operator, and $\{\cdot\}$ extracts the fractional component by discarding the integer part. The phase shift $T/4$ centers the triangle wave symmetrically around zero, which will be convenient for subsequent Fourier analysis.

Fourier Approximation. Since the rotated rounding function $f(t)$ is periodic and square-integrable, it admits a Fourier series expansion. Applying the Fourier transformation on Equation 7, we obtain the following closed-form Fourier approximation:

$$f(t) \approx -A \sum_{m=0}^{\infty} \frac{(-1)^m}{(2m+1)^2} \sin((2m+1)\sqrt{2}\pi t), \quad (8)$$

where $(2m+1)\sqrt{2}\pi$ denotes the angular frequency of the m -th sinusoid term. The scalar A is an amplitude coefficient, as illustrated in Figure 2, which controls the sharpness of the resulting curve. Notably, **instead of fixing A to**

the vanilla Fourier amplitude $A = 2\sqrt{2}/\pi^2$, we treat it as a tunable parameter. An appropriate choice of A can yield improved training stability and optimization behavior, whereas an improper choice may lead to gradient vanishing or explosion; see Section 3.2 for a detailed discussion.

We further consider a truncated Fourier approximation as

$$f_M(t) = -A \sum_{m=0}^M \frac{(-1)^m}{(2m+1)^2} \sin((2m+1)\sqrt{2}\pi t), \quad (9)$$

where M refers to the order of Fourier approximation. Higher-order terms encode finer structural details of the rounding operator but incur increasing computational cost.

Inverse Rotation. To employ the rotated Fourier approximation as a gradient surrogate, we map the smooth function $f(t)$ back to the original coordinates (x, x_q) . Based on the coordinate transformation in (6), the Fourier expansion of $f(t)$, and the chain rule, the general form of the rotated damped Fourier surrogate (RDFS) for the rounding operator can be expressed as

$$\frac{\partial x_q}{\partial x} = \frac{1 - A\sqrt{2}\pi \sum_{m=0}^M \frac{(-1)^m}{2m+1} \cos((2m+1)\pi(x+x_q))}{1 + A\sqrt{2}\pi \sum_{m=0}^M \frac{(-1)^m}{2m+1} \cos((2m+1)\pi(x+x_q))}. \quad (10)$$

In practice, we retain only the first-order term ($M = 0$), which provides an effective trade-off between approximation fidelity and negligible computational overhead. Under this setting, the RDFS in Equation 10 reduces to its first-order form as Equation 5. A complete derivation of the RDFS is provided in Appendix B.

3.2. Damped Amplitude and Gradient Stabilization

The choice of the amplitude parameter A requires careful consideration, as it directly governs the trade-off between approximation fidelity and optimization stability.

Role of Amplitude. The amplitude A controls the sharpness of the rotated Fourier surrogate and determines how closely it approximates the true rounding operator. When A is small (approaching the STE case as $A \rightarrow 0$), the surrogate is overly smooth, which weakens its ability to capture the fine-grained structure of rounding and leads to biased or ineffective gradient signals. Increasing A (while remaining within the admissible range implied by the Fourier construction) improves approximation accuracy by bringing the surrogate closer to hard rounding. However, as the surrogate sharpens, it progressively inherits the pathological optimization behavior of the true rounding operator: gradients vanish over large regions and become highly unstable in the vicinity of discontinuities, resulting in gradient vanishing or explosion. This intrinsic trade-off motivates the use of a damped amplitude that balances expressiveness and numerical stability.

Well-Conditioned Surrogate Region. Our analysis reveals the existence of an *ill-conditioned amplitude regime* in which the rotated Fourier surrogate becomes nearly tangential to horizontal plateaus as A approaches $1/(\sqrt{2}\pi)$, leading to severely attenuated gradients. To avoid this failure mode, our design explicitly excludes this region. As shown in the amplitude sensitivity study in Figure 8, this ill-conditioned regime manifests as a pronounced performance “well” in empirical results, which closely aligns with the theoretical conditioning analysis. This consistency between theory and observation provides strong evidence that a proper amplitude choice can fundamentally improve optimization gain and avoid potential instability.

Practical Amplitude Selection. Although Fourier analysis suggests a theoretically admissible amplitude of $A = \frac{2\sqrt{2}}{\pi^2}$, strictly adhering to this value is suboptimal in practice for large-scale LLM training due to the aforementioned conditioning issues. We therefore treat A as a **damped and tunable parameter**. In all experiments, we select a default value of $A = 0.21$, which lies safely outside the ill-conditioned regime while still capturing sufficient structural information of the rounding operator to yield effective gradient signals. This choice provides a stable and robust operating point across models and training settings. While more sophisticated strategies such as dynamically evolving A during training, may further improve performance, we leave such curriculum-based designs as an interesting direction for future work.

4. Theoretical and Efficiency Analysis

4.1. Theoretical Comparison with STE

We compare STE and StableQAT using surrogate approximations of the rotated rounding function (7). By periodicity, we may focus on a single period $[0, T]$ without loss of generality. As the rotated function is square-integrable, we conduct our analysis in the space $L^2([0, T])$.

Theorem 4.1. Let $f \in L^2([0, T])$ and let f_n be the n th partial Fourier sum of f . Then, for all $n \in \mathbb{N}$,

- (i) f_n is the unique minimizer of the L^2 approximation error among trigonometric polynomials of degree at most n ;
- (ii) For $n \geq 1$, $\|f - f_n\|_2 < \|f - f_0\|_2$ if and only if f is non-constant almost everywhere.

Proof. See Appendix C. \square

Remark I. Theorem 4.1(i) implies that the n th partial Fourier sum is the optimal L^2 surrogate of the rotated rounding function among trigonometric polynomials of degree at most n . For STE, the surrogate is restricted to constant functions. In contrast, StableQAT admits surrogates from trigonometric polynomials of degree at most $n \in \mathbb{N}$, making STE a special case of StableQAT with $n = 0$.

Remark II. Theorem 4.1(ii) implies that, unless the function is constant almost everywhere, its surrogate drawn from trigonometric polynomials of degree at least 1 achieves a strictly smaller L^2 approximation error than those restricted to constant functions. Consequently, StableQAT admits surrogate functions that are provably closer to the rotated rounding function than STE in the L^2 sense.

4.2. Theoretical Comparison with DSQ

We then compare DSQ and StableQAT in terms of gradient stability by analyzing the statistical properties of their surrogate gradients under uniform sampling over the clipping range. Our analysis focuses on the asymptotic regime in which the surrogate function closely approximates the rounding function. Such setting is particularly relevant for low-bit QAT (2–4 bits), where accurately capturing discrete quantization effects is critical.

Theorem 4.2. Let $g_{\text{DSQ}}(\cdot; \alpha)$ and $g_{\text{StableQAT}}(\cdot; A)$ be the gradient surrogates of DSQ and StableQAT, parameterized by $\alpha > 0$ and $A \in (0, \frac{1}{\sqrt{2}\pi})$, respectively. Let random variable ξ be uniformly distributed on the interval $[l, u]$, i.e., $\xi \sim U(l, u)$. Consider the asymptotic regimes in which the surrogate functions move close to the rounding function. Then, the limits of the expectations satisfy

$$\lim_{\alpha \rightarrow 0^+} \mathbb{E}_{\xi \sim U(l, u)}[g_{\text{DSQ}}(\xi; \alpha)] = 1,$$

$$\lim_{A \rightarrow (\frac{1}{\sqrt{2}\pi})^-} \mathbb{E}_{\xi \sim U(l, u)}[g_{\text{StableQAT}}(\xi; A)] = \frac{4}{\pi} - 1,$$

and the limits of the variances satisfy

$$\lim_{\alpha \rightarrow 0^+} \text{Var}_{\xi \sim U(l, u)}[g_{\text{DSQ}}(\xi; \alpha)] = \infty,$$

$$\lim_{A \rightarrow (\frac{1}{\sqrt{2}\pi})^-} \text{Var}_{\xi \sim U(l, u)}[g_{\text{StableQAT}}(\xi; A)] = \frac{16}{3\pi} - \frac{16}{\pi^2}.$$

Proof. See Appendix D. \square

Remark I. In Theorem 4.2, $g_{\text{StableQAT}}(\cdot; A)$ is derived using the first-order Fourier partial sum of the rotated rounding function. Although StableQAT allows higher-order Fourier partial sums, we focus on the first-order case as it is the variant used in our experiments and suffices to reveal the differences in gradient stability.

Remark II. Theorem 4.2 shows that DSQ’s gradient variance diverges as it sharpens towards the rounding function, whereas the periodic structure of StableQAT maintains bounded variance (≈ 0.076) at maximum sharpness. This distinction directly impacts training stability: bounded variance ensures consistent gradient magnitudes, while divergent variance may cause gradient explosion. Thus, gradient stability is a key advantage of StableQAT over DSQ in low-bit QAT regimes.

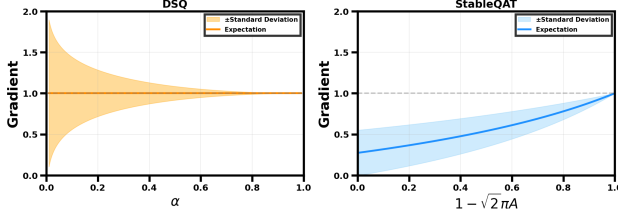


Figure 3. Gradient spread of DSQ and StableQAT. As the surrogate sharpens toward rounding operator, DSQ exhibits exploding variance, while StableQAT shows bounded variance.

4.3. Efficiency Comparison

We further show that RDFS achieves nearly identical computational efficiency to STE, while being several times faster and more lightweight than DSQ. This makes StableQAT a plug-and-play surrogate for a wide range of QAT pipelines, providing consistent performance gains without additional computational or memory cost.

Computational Efficiency: `cosine` vs. `exp`. Soft quantization methods such as DSQ (Gong et al., 2019) and SigmoidQuant (Semenov, 2025) approximate rounding using sigmoid or `tanh`, which rely on expensive exponential evaluations. On modern hardwares, `exp` typically requires high-order polynomial approximation, and numerical-stability handling, leading to high latency and register pressure (Muller et al., 2018; NVIDIA, 2024).

In contrast, trigonometric functions like `cosine` and `sine` operate on bounded inputs, admit lower-degree polynomial approximations, and avoid saturation handling. Consequently, RDFS exhibits lower and more predictable execution cost, which is especially beneficial in QAT where surrogate gradients are repeatedly evaluated.

RDFS is Fusion-Friendly. RDFS consists only of elementary arithmetic and a single trigonometric operation, without auxiliary states or annealing schedules. Its low register footprint and branch-free structure make it well suited for kernel fusion in modern deep learning runtimes, e.g., PyTorch (Imambi et al., 2021), CUDA (NVIDIA, 2024), and Triton (Tillet et al., 2019).

Negligible Computational Overhead. We benchmark RDFS on LLaMA-3-1B with batch size 4 and sequence length 128. As shown in Figure 4, StableQAT matches STE in backward-pass latency and memory usage, while being up to 5× more efficient than `exp`-based surrogate like DSQ.

5. Experiments

We comprehensively evaluate StableQAT from three complementary perspectives: (i) model performance, (ii) training

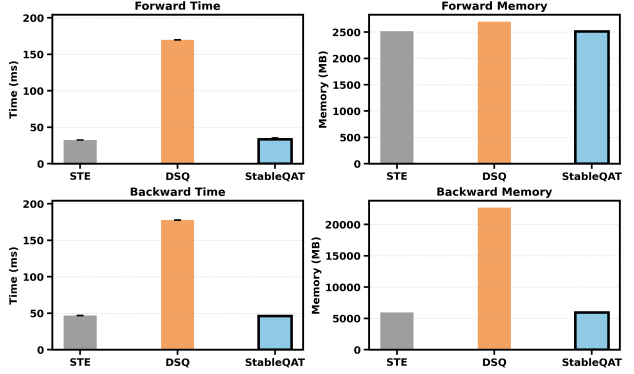


Figure 4. Time and space cost comparison (lower is better). They are measured on an input tensor with batch size 4 and sequence length 128. Each method is repeated 20 times.

ing stability, and (iii) ablation studies that reveal the impact of key design choices. Our experiments span both Large Language Models (LLMs) and Vision Transformers (ViTs) in Appendix ??, demonstrating the generality, effectiveness, and robustness of StableQAT across scenarios.

5.1. Large Language Model

Experiment Setup. Similarly to ParetoQ, we evaluate two representative LLMs, LLaMA-3-1B and LLaMA-3-3B (Meta, 2024), under weight-only quantization at 2–4 bit precision. Model performance is assessed on a popular suite of benchmarks, including ARC-Easy, ARC-Challenge, BoolQ, HellaSwag, OpenBookQA, PIQA, SciQ, Winogrande, using the lm-evaluation-harness (Gao et al., 2024). We compare against the recent LLM-QAT method ParetoQ and the representative soft-rounding approach DSQ, both reproduced from their official repositories with recommended hyperparameters and training schedules. The training corpus is constructed by mixing SlimPajama (Soboleva et al., 2023) and FineWeb-Edu (Penedo et al., 2024) at a one-by-one ratio, while varying the total token budget across experiments.

Results on LLaMA-3-1B. Across all evaluated bitwidths (2–4 bits), StableQAT consistently outperforms both ParetoQ and DSQ, as shown in Table 2, achieving improvements of up to **6.88%** under different training recipes. At **4 bits**, StableQAT delivers the best overall performance, surpassing ParetoQ and DSQ by **0.25%–1.38%**, and in several settings even exceeding the FP16 baseline. The advantage becomes substantially more pronounced at **3 bits**, where StableQAT consistently improves over both baselines by **2.70%–6.88%**, highlighting its effectiveness in the regime where QAT noise becomes severe. Under the most challenging **2-bit** setting, StableQAT remains stable and achieves higher performance by **1.69%**, while ParetoQ and DSQ face more variance or training collapse (Figure 6).

StableQAT: Stable, High-Performing, Efficient QAT

Table 2. LLaMA-3.2-1B results. StableQAT at 4-bit outperforms the 16-bit baseline, while 3-bit StableQAT remains competitive.

Bits	Method	Setting	Arc-e	Arc-c	Boolq	Hellaswag	Openbookqa	Piqa	SciQ	Winogrande	Avg	Δ
16	Baseline	Baseline	60.61	36.01	63.70	63.78	36.60	74.43	88.40	60.06	60.45	–
4	Baseline no QAT	Baseline no QAT	43.31	27.05	52.57	46.75	31.20	65.83	78.00	53.12	49.73	–
4	ParetoQ	10B Tokens & lr=1e-5	59.89	30.97	59.27	56.07	34.40	71.65	88.80	56.83	57.24	–
4	DSQ	10B Tokens & lr=1e-5	55.01	31.66	61.16	55.75	34.20	71.87	86.00	56.27	56.49	–
4	StableQAT	10B Tokens & lr=1e-5	60.48	32.17	62.02	56.54	32.60	72.63	89.60	56.91	57.87	+1.38
4	ParetoQ	20B Tokens & lr=1e-4	65.49	36.86	63.82	61.22	39.40	74.70	86.70	59.51	60.96	–
4	DSQ	20B Tokens & lr=1e-4	65.45	37.37	63.73	62.04	39.40	74.16	86.40	59.98	61.07	–
4	StableQAT	20B Tokens & lr=1e-4	65.74	37.54	64.01	61.15	40.00	74.59	86.4	60.46	61.24	+0.25
3	Baseline no QAT	Baseline no QAT	24.74	26.30	40.64	26.11	29.00	50.49	24.90	48.30	33.81	–
3	ParetoQ	10B Tokens & lr=1e-5	30.85	22.10	48.53	29.19	27.80	55.33	50.30	47.28	38.92	–
3	DSQ	10B Tokens & lr=1e-5	29.88	23.63	46.27	29.31	28.00	53.86	46.90	48.54	38.30	–
3	StableQAT	10B Tokens & lr=1e-5	38.55	23.98	59.24	33.14	27.00	59.63	67.70	52.17	45.18	+6.88
3	ParetoQ	20B Tokens & lr=2e-4	35.69	64.24	61.23	58.91	37.40	73.32	87.50	58.27	59.57	–
3	DSQ	20B Tokens & lr=2e-4	32.85	60.77	59.76	56.21	36.6	72.42	83.10	57.62	57.42	–
3	StableQAT	20B Tokens & lr=2e-4	36.43	64.06	63.24	59.49	37.80	73.67	86.7	59.59	60.12	+2.70
2	ParetoQ	30B Tokens & lr=1e-4	60.02	34.22	57.65	55.63	35.80	72.91	82.90	59.19	57.29	–
2	DSQ	30B Tokens & lr=1e-4	59.13	32.59	58.72	55.65	36.20	72.03	80.50	56.27	56.39	–
2	StableQAT	30B Tokens & lr=1e-4	61.53	32.94	63.00	56.24	37.40	72.63	83.10	57.77	58.08	+1.69

Results on LLaMA-3-3B. We observe consistent and often amplified trends on the larger LLaMA-3-3B model, as reported in Table 3, indicating that the benefits of StableQAT scale favorably with model size. Across all 2–4 bit settings, StableQAT uniformly outperforms ParetoQ and DSQ, achieving gains of up to **2.67** at **4 bits** and **2.38%** at **3 bits**. Notably, the **4-bit** StableQAT model surpasses the FP16 baseline, while the **3-bit** configuration reaches near full-precision performance, demonstrating that aggressive quantization can be achieved without sacrificing accuracy on larger models. Even at **2 bits**, where optimization is particularly fragile, StableQAT maintains stable training dynamics and competitive performance. These results confirm that StableQAT provides a scalable and robust solution for ultra-low-bit QAT of large language models.

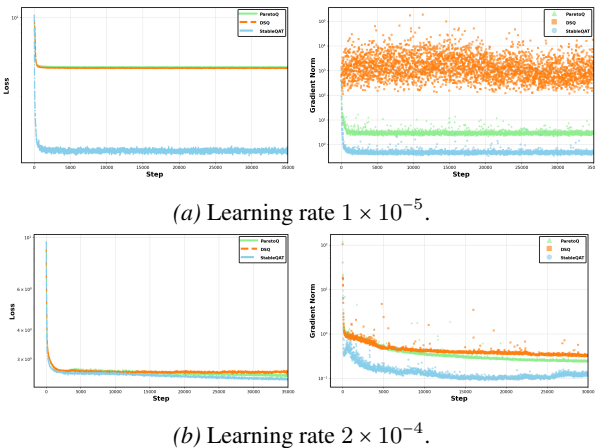


Figure 5. Training loss (left) and gradient norm (right) comparison for Llama-3-1B under different learning rates.

5.2. Training Stability Validation

Gradient Dynamics and Convergence Behavior. Figure 5 provides a clear empirical validation of our theoretical analysis in Section 4. StableQAT exhibits smooth and well-behaved optimization dynamics across learning rates, with steadily decreasing training loss and controlled gradient norms throughout training. This behavior is consistent with Theorem 4.1, which shows that our rotated damped Fourier surrogate achieves strictly smaller approximation error to the rotated rounding function than STE, resulting in a more faithful optimization direction and improved convergence. Moreover, StableQAT maintains reliable and substantial gradient signals while effectively eliminating extreme gradient outliers. In contrast to DSQ, which typically display sharp gradient spikes and outliers inducing instability. The phenomenon is well aligned with Theorem 4.2, the gradient variance of StableQAT remains bounded, leading to gradual gradient-norm decay rather than explosion or premature vanishing. Together, these properties enable StableQAT to converge to lower loss values and better optimum, demonstrating that its theoretical advantages translate directly into stable and reliable training behavior in practice.

Performance Error Bar.

The performance error bars in Figure 6 characterize training robustness across multiple random seeds and learning-rate settings. For each method and bit-width, we report the mean performance together with its dispersion, thereby capturing

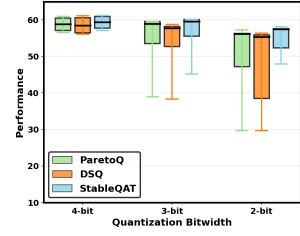


Figure 6. Performance error bar for LLaMA-3-1B across a shared hyperparameter set.

Table 3. LLaMA-3.2-3B results. StableQAT at 4-bit outperforms the 16-bit baseline, while 3-bit StableQAT remains competitive.

Bits	Method	Setting	Arc-e	Arc-c	Boolq	Hellaswag	Openbookqa	Piqa	SciQ	Winogrande	Avg	Δ
16	Baseline	Baseline	71.63	45.99	73.39	73.61	43.00	77.48	92.70	69.85	68.46	–
4	Baseline no QAT	Baseline no QAT	61.99	37.63	68.44	66.87	36.40	74.48	89.40	61.96	62.15	–
4	ParetoQ	20B Tokens & lr=1e-4	71.83	45.48	70.13	71.20	42.40	76.58	90.60	66.25	66.81	–
4	DSQ	20B Tokens & lr=1e-4	70.19	41.73	68.39	64.58	39.40	76.51	90.93	64.40	64.48	–
4	StableQAT	20B Tokens & lr=1e-4	72.05	44.97	70.21	71.28	42.00	77.58	91.50	67.64	67.15	+2.67
3	Baseline no QAT	Baseline no QAT	26.14	25.43	44.01	26.61	28.40	52.50	26.00	49.01	34.76	–
3	ParetoQ	20B Tokens & lr=1e-4	71.47	45.16	70.28	70	42	76.15	91	65.93	66.50	–
3	DSQ	20B Tokens & lr=1e-4	66.58	41.64	70.24	66.58	40.60	76.28	89.80	64.48	64.52	–
3	StableQAT	20B Tokens & lr=1e-4	71.04	44.97	69.02	70.81	44.00	78.29	90.4	66.69	66.90	+2.38
2	Baseline no QAT	Baseline no QAT	25.55	24.91	43.88	26.03	28.80	53.26	21.40	48.30	34.02	–
2	ParetoQ	30B Tokens & lr=1e-4	65.73	38.08	65.73	64.13	39.40	74.68	84.30	61.43	61.69	–
2	DSQ	30B Tokens & lr=1e-4	69.19	40.78	65.54	66.03	41.60	74.92	88.60	63.61	63.78	–
2	StableQAT	30B Tokens & lr=1e-4	68.48	40.87	63.06	65.20	41.00	75.41	87.00	63.38	63.05	+1.36

sensitivity to optimization noise beyond single-run best results. StableQAT consistently achieves the highest mean performance with the tightest error bars, indicating reliable convergence under different hyperparameter perturbations, with the margin becoming more pronounced at lower bit-widths where optimization is particularly fragile. In contrast, ParetoQ exhibits both lower mean performance and larger variance. Its relies on the STE, which does not capture the intrinsic structure of the rounding operator, often yields noisy and misleading update directions. These misaligned gradients can push weights across quantization thresholds in an uncontrolled manner, increasing sensitivity, sometimes leading to training collapse. DSQ shows elevated variance for a different reason. Its sigmoid-style surrogate introduces regions of extremely large gradients near the transition boundaries. Such gradient explosion amplifies small perturbations during training, making optimization sensitive and introducing widened error bars.

5.3. Ablation Studies

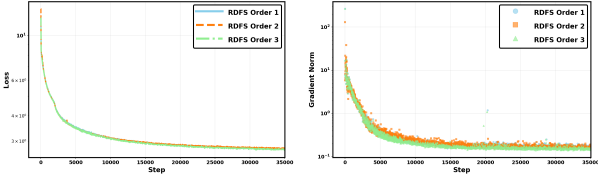


Figure 7. Training loss and gradient norm dynamics across RDFS’s order $M = 0, 1, 2$.

Fourier Order of RDFS. We study the effect of Fourier truncation order M in RDFS. Figure 7 compares training dynamics across $M = 0, 1, 2$. A first-order approximation ($M = 0$) already captures the majority of the performance and stability gains, yielding smooth loss decay and well-controlled gradient norms. While higher-order terms introduce finer structural details of the quantization operator, their empirical benefits are marginal and come at increased numerical complexity. These observations

well validate our design choice of adopting the first-order RDFS as Equation 5, which offers an effective balance between approximation fidelity, training stability, and computational simplicity for quantization-aware training.

Amplitude. We next vary the amplitude A to control the sharpness of surrogate gradient, to empirically validate the damped amplitude design predicted by the theoretical analysis in Section 3.2. As shown in Figure 8, the empirical results closely align with the theoretical characterization and clearly reveal the presence of an ill-conditioned regime, where the surrogate curves become nearly tangential to horizontal plateaus. In contrast, moderate amplitude values provide a favorable balance between approximation fidelity and optimization stability. In particular, the selected setting $A = 0.21$ consistently achieves stronger performance, benefiting from an adequate approximation of the rounding operator while maintaining stable and well-conditioned training dynamics.

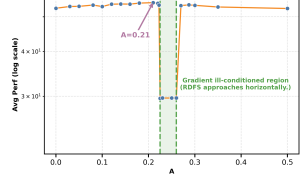


Figure 8. Performance of 3-bit Llama-3.2-1B across different amplitudes.

6. Conclusion

We propose StableQAT to address the training instability and suboptimal performance of quantization-aware training. StableQAT employs a rotated damped Fourier surrogate (RDFS) that captures the intrinsic structure of quantization while avoiding the gradient instability of conventional soft-quantization. We provide theoretical guarantees showing that RDFS ensures bounded gradient variance and preserves admissible gradient magnitudes, enabling stable and effective optimization. Extensive experiments on LLMs and ViTs demonstrate consistent improvements in both peak and average performance under low-bit QAT.

References

Ahn, M. and Yoo, S. Differentiable, stable and efficient floating-point quantization. *OpenReview (ICLR 2026 submission; withdrawn)*, 2025.

Bai, R., Liu, B., and Liu, Q. Skim: Any-bit quantization pushing the limits of post-training quantization. In *Proceedings of the 42nd International Conference on Machine Learning (ICML)*, 2025.

Bengio, Y., Léonard, N., and Courville, A. Estimating or propagating gradients through stochastic neurons for conditional computation. *arXiv preprint arXiv:1308.3432*, 2013a.

Bengio, Y., Léonard, N., and Courville, A. Estimating or propagating gradients through stochastic neurons for conditional computation. *arXiv preprint arXiv:1308.3432*, 2013b.

Bulat, A., Ouali, Y., and Tzimiropoulos, G. Qbb: Quantization with binary bases for llms. In *Advances in Neural Information Processing Systems (NeurIPS)*, 2024.

Chen, M., Shao, W., Xu, P., Wang, J., Gao, P., Zhang, K., and Luo, P. Efficientqat: Efficient quantization-aware training for large language models. In *Proceedings of the 63rd Annual Meeting of the Association for Computational Linguistics (ACL)*, 2025.

Choi, J., Wang, Z., Venkataramani, S., Chuang, P. I., Srinivasan, V., and Gopalakrishnan, K. Pact: Parameterized clipping activation for quantized neural networks. In *International Conference on Learning Representations (ICLR)*, 2018.

Défossez, A., Adi, Y., and Synnaeve, G. Differentiable model compression via pseudo quantization noise. *Transactions on Machine Learning Research (TMLR)*, 2022.

Ding, T., Chen, T., Zhu, H., Jiang, J., Zhong, Y., Zhou, J., Wang, G., Zhu, Z., Zharkov, I., and Liang, L. The efficiency spectrum of large language models: An algorithmic survey. *arXiv preprint arXiv:2312.00678*, 2023.

Du, D., Zhang, Y., Cao, S., Guo, J., Cao, T., Chu, X., and Xu, N. Bitdistiller: Unleashing the potential of sub-4-bit llms via self-distillation. In *Proceedings of the 62nd Annual Meeting of the Association for Computational Linguistics (ACL)*, 2024a.

Du, D., Zhang, Y., Cao, S., Guo, J., Cao, T., Chu, X., and Xu, N. Bitdistiller: Unleashing the potential of sub-4-bit llms via self-distillation. In *Annual Meeting of the Association for Computational Linguistics (ACL)*, 2024b.

Esser, S. K., McKinstry, J. L., Bablani, D., Appuswamy, R., and Modha, D. S. Learned step size quantization. *arXiv preprint arXiv:1902.08153*, 2019.

Frantar, E., Ashkboos, S., Hoefer, T., and Alistarh, D. Gptq: Accurate post-training quantization for generative pre-trained transformers. In *International Conference on Learning Representations (ICLR)*, 2023.

Gao, L., Tow, J., Abbasi, B., Biderman, S., Black, S., DiPofi, A., Foster, C., Golding, L., Hsu, J., Le Noac'h, A., Li, H., McDonell, K., Muennighoff, N., Ociepa, C., Phang, J., Reynolds, L., Schoelkopf, H., Skowron, A., Sutawika, L., Tang, E., Thite, A., Wang, B., Wang, K., and Zou, A. The language model evaluation harness, 07 2024. URL <https://zenodo.org/records/12608602>.

Gong, R., Liu, X., Jiang, S., Li, T., Hu, P., Lin, J., Yu, F., and Yan, J. Differentiable soft quantization: Bridging full-precision and low-bit neural networks. In *Proceedings of the IEEE/CVF International Conference on Computer Vision (ICCV)*, 2019.

Gradshteyn, I. S. and Ryzhik, I. M. *Table of integrals, series, and products*. Academic press, 2007.

Huang, X., Shen, Z., Li, S., Liu, Z., Hu, X., Wicaksana, J., Xing, E., and Cheng, K.-T. Sdq: Stochastic differentiable quantization with mixed precision. In *Proceedings of the 39th International Conference on Machine Learning (ICML)*, 2022.

Hubara, I., Courbariaux, M., Soudry, D., El-Yaniv, R., and Bengio, Y. Quantized neural networks: Training neural networks with low precision weights and activations. *Journal of Machine Learning Research (JMLR)*, 18(187):1–30, 2018.

Imam, S., Prakash, K. B., and Kanagachidambaresan, G. Pytorch. In *Programming with TensorFlow: solution for edge computing applications*, pp. 87–104. Springer, 2021.

Jacob, B., Kligys, S., Chen, B., Zhu, M., Tang, M., Howard, A., Adam, H., and Kalenichenko, D. Quantization and training of neural networks for efficient integer-arithmetic-only inference. In *Proceedings of the IEEE Conference on Computer Vision and Pattern Recognition (CVPR)*, 2018.

Kundu, A., Yoo, C., Cho, M., and Adya, S. Differentiable soft min-max loss to restrict weight range for model quantization. 2nd Differentiable Almost Everything Workshop at ICML 2024, 2024.

Li, Y., Yu, Y., Liang, C., He, P., Karampatziakis, N., Chen, W., and Zhao, T. Loftq: Lora-fine-tuning-aware quantization for large language models. In *International Conference on Learning Representations (ICLR)*, 2024.

Liu, Z., Oguz, B., Zhao, C., Chang, E., Stock, P., Mehdad, Y., Shi, Y., Krishnamoorthi, R., and Chandra, V. LLM-QAT: Data-free quantization aware training for large language models. In *Findings of the Association for Computational Linguistics: ACL 2024*, 2024a.

Liu, Z., Oguz, B., Zhao, C., Chang, E., Stock, P., Mehdad, Y., Shi, Y., Krishnamoorthi, R., and Chandra, V. Llm-qat: Data-free quantization aware training for large language models. In *Findings of the Association for Computational Linguistics: ACL 2024*, 2024b.

Liu, Z., Zhao, C., Huang, H., Chen, S., Zhang, J., Zhao, J., Roy, S., Jin, L., Xiong, Y., Shi, Y., Xiao, L., Tian, Y., Soran, B., Krishnamoorthi, R., Blankevoort, T., and Chandra, V. Paretoq: Improving scaling laws in extremely low-bit llm quantization. *arXiv*, 2025.

Meta. The llama 3 herd of models, 2024. URL <https://arxiv.org/abs/2407.21783>.

Muller, J.-M., Brisebarre, N., De Dinechin, F., Jeannerod, C.-P., Lefevre, V., Melquiond, G., Revol, N., Stehlé, D., Torres, S., et al. *Handbook of floating-point arithmetic*, volume 1. Springer, 2018.

NVIDIA. Cuda c++ programming guide, 2024.

Panferov, A., Chen, J., Tabesh, S., Castro, R. L., Nikdan, M., and Alistarh, D. Quest: Stable training of llms with 1-bit weights and activations. In *International Conference on Machine Learning (ICML)*, 2025.

Penedo, G., Kydlíček, H., allal, L. B., Lozhkov, A., Mitchell, M., Raffel, C., Werra, L. V., and Wolf, T. The fineweb datasets: Decanting the web for the finest text data at scale, 2024. URL <https://arxiv.org/abs/2406.17557>.

Qin, H., Ma, X., Zheng, X., Li, X., Zhang, Y., Liu, S., Luo, J., Liu, X., and Magno, M. Accurate lora-finetuning quantization of llms via information retention. In *Proceedings of the 41st International Conference on Machine Learning (ICML)*, 2024.

Salishev, S. and Akhremchik, I. Gdnsq: Gradual differentiable noise scale quantization for low-bit neural networks. *arXiv*, 2025.

Semenov, S. Smooth approximations of the rounding function. *arXiv preprint arXiv:2504.19026*, 2025.

Soboleva, D., Al-Khateeb, F., Myers, R., Steeves, J. R., Hestness, J., and Dey, N. SlimPajama: A 627B token cleaned and deduplicated version of RedPajama. <https://cerebras.ai/blog/slimpajama-a-627b-token-cleaned-and-deduplicated-2023>. URL <https://huggingface.co/datasets/cerebras/SlimPajama-627B>.

Stein, E. M. and Shakarchi, R. *Fourier analysis: an introduction*, volume 1. Princeton University Press, 2011.

Tillet, P., Kung, H.-T., and Cox, D. Triton: an intermediate language and compiler for tiled neural network computations. In *Proceedings of the 3rd ACM SIGPLAN International Workshop on Machine Learning and Programming Languages*, pp. 10–19, 2019.

van Breugel, B., Bondarenko, Y., Whatmough, P., and Nagel, M. Fptquant: Function-preserving transforms for llm quantization. *arXiv*, 2025.

Vlassis, G., Ashkboos, S., Volkova, A., Hoefer, T., and Al-istarth, D. Beyond outliers: A study of optimizers under quantization. *arXiv*, 2025.

Xiao, G., Lin, J., Seznec, M., Wu, H., Demouth, J., and Han, S. Smoothquant: Accurate and efficient post-training quantization for large language models. In *International Conference on Machine Learning (ICML)*, 2023.

Zhong, Z., Chen, T., and Wang, Z. Mat: mixed-strategy game of adversarial training in fine-tuning. *arXiv preprint arXiv:2306.15826*, 2023.

A. Related Work

Recent works on post-training quantization (PTQ) focus on mitigating outliers and distribution skewness, which become increasingly problematic at lower bitwidths. Techniques such as function-preserving transformations and channel-wise clustering aim to reshape weight distributions so that uniform or centroid-based quantizers incur less error without modifying model parameters (van Breugel et al., 2025; Bai et al., 2025).

Quantization-aware training (QAT) addresses PTQ’s limitations by incorporating quantization effects into training; however, as bitwidth decreases, STE-based training often becomes unstable or biased. Several works focus on improving training efficiency and scalability of QAT rather than altering the quantization operator itself; examples include block-wise or staged training schemes that reduce computational cost, as well as data-free distillation strategies that remove dependence on large calibration datasets (Liu et al., 2024b; Chen et al., 2025). Another thread leverages self-distillation objectives to stabilize sub-4-bit settings (Du et al., 2024a).

A complementary line of work reformulates quantization as an approximation or decomposition problem. For instance, QBB represents weights as linear combinations of binary bases, replacing multiplications with additions while optimizing scales via distillation (Bulat et al., 2024). LoRA-aware approaches such as LoftQ and IR-QLoRA integrate quantization with low-rank adaptation, either by alternating between quantization and decomposition or by explicitly preserving information through auxiliary connections (Li et al., 2024; Qin et al., 2024). These methods improve efficiency and flexibility but still depend on standard rounding behavior and STE-style gradients. Another body of work treats quantization through stochastic or noise-based perspectives, aiming to avoid hard discrete operators during training such as DiffQ which introduces pseudo quantization noise to approximate quantization effects (Défossez et al., 2022). Similarly, stochastic differentiable quantization frameworks have bitwidths sampled probabilistically and optimized via reparameterization (Huang et al., 2022).

Differentiable and soft quantization methods more directly target the rounding operation by introducing continuous relaxations. DSQ is a representative example, utilizing parameterized smooth function whose sharpness increases during training (Gong et al., 2019). DSMM (Kundu et al., 2024) introduces a differentiable soft min–max loss to reduce weight ranges by making max/min approximations differentiable and learnable.

Recent work pushes differentiable quantization further by explicitly optimizing bitwidths or noise scales as continuous variables. GDNSQ (Salishev & Akhremchik, 2025) frames quantization as a smooth constrained optimization over effective bitwidths, combining STE-style estimators with gradual noise scheduling and distillation losses. Floating-point oriented frameworks (Ahn & Yoo, 2025) extend pseudo-quantization training to mixed floating-point formats, enabling differentiable optimization of mantissa and exponent precisions. Other works provide scaling laws and diagnostics to assess failure modes at low-bit regimes (Liu et al., 2025; Vlassis et al., 2025). However, a key challenge in low-bit QAT that remains lies in reconciling discrete inference with stable, informative gradients.

B. Rotated Damped Fourier Surrogate Derivation

Fourier series derivation. We first derive the Fourier series expansion of the zig-zag function (7) written as

$$f(t) = \frac{1}{2\sqrt{2}} \left(1 - 4 \left| r(t) - \frac{1}{2} \right| \right),$$

where $r(t) = \left\{ \frac{t-T/4}{T} \right\}$, $T = \sqrt{2}$ is the period, and $\{\cdot\}$ denotes the fractional part function. Since $f(t)$ is square integrable and periodic, it admits a Fourier series (Stein & Shakarchi, 2011):

$$f(t) = a_0 + \sum_{k=1}^{\infty} \left[a_k \cos\left(\frac{2\pi k t}{T}\right) + b_k \sin\left(\frac{2\pi k t}{T}\right) \right].$$

Due to the phase shift by $T/4$ in the definition of $r(t)$, the function $f(t)$ is odd, i.e., $f(-t) = -f(t)$. Consequently, $a_k = 0$ for all $k \in \mathbb{N}$, leaving only sine terms:

$$f(t) = \sum_{k=1}^{\infty} b_k \sin\left(\frac{2\pi k}{T} t\right).$$

The Fourier coefficients, computed via $b_k = \frac{2}{T} \int_0^T f(t) \sin\left(\frac{2\pi k t}{T}\right) dt$, are given by for all $m \in \mathbb{N}$,

$$b_{2m+1} = -\frac{2\sqrt{2}}{\pi^2} \cdot \frac{(-1)^m}{(2m+1)^2}, \quad b_{2m+2} = 0.$$

Thus, only odd harmonics contribute, and the zig-zag function admits the sine-series expansion

$$f(t) = -\frac{2\sqrt{2}}{\pi^2} \sum_{m=0}^{\infty} \frac{(-1)^m}{(2m+1)^2} \sin((2m+1)\sqrt{2}\pi t).$$

To obtain a tunable surrogate, we replace the fixed amplitude $\frac{2\sqrt{2}}{\pi^2}$ with a learnable parameter A :

$$f(t) = -A \sum_{m=0}^{\infty} \frac{(-1)^m}{(2m+1)^2} \sin((2m+1)\sqrt{2}\pi t),$$

with derivative

$$f'(t) = -A\sqrt{2}\pi \sum_{m=0}^{\infty} \frac{(-1)^m}{2m+1} \cos((2m+1)\sqrt{2}\pi t). \quad (11)$$

Rotation to the rounding function. The key observation is that rotating the zig-zag function by 45° counterclockwise yields the staircase rounding function. To see this, we apply the standard rotation matrix to each point $(t, f(t))$ on the graph:

$$\begin{pmatrix} x \\ x_q \end{pmatrix} = \frac{1}{\sqrt{2}} \begin{pmatrix} 1 & -1 \\ 1 & 1 \end{pmatrix} \begin{pmatrix} t \\ f(t) \end{pmatrix} = \begin{pmatrix} t - f(t) \\ t + f(t) \end{pmatrix}^T, \quad (12)$$

where x represents the input and x_q represents the quantized (rounded) output. Inverting this relationship gives $t = (x + x_q)/\sqrt{2}$.

Gradient surrogate derivation. Using the parameterization in Equation (12) and the chain rule, we have

$$\frac{\partial x_q}{\partial x} = \frac{\partial x_q / \partial t}{\partial x / \partial t} = \frac{1 + f'(t)}{1 - f'(t)}. \quad (13)$$

Substituting the Fourier series derivative from Equation (11) and using $t = (x + x_q)/\sqrt{2}$, we obtain

$$\frac{\partial x_q}{\partial x} = \frac{1 - A\sqrt{2}\pi \sum_{m=0}^{\infty} \frac{(-1)^m}{2m+1} \cos((2m+1)\pi(x + x_q))}{1 + A\sqrt{2}\pi \sum_{m=0}^{\infty} \frac{(-1)^m}{2m+1} \cos((2m+1)\pi(x + x_q))}.$$

C. Proof of Theorem 4.1

For clarity in the proof, we restate Theorem 4.1 using precise mathematical notation.

Theorem C.1. *Let $f \in L^2([0, T])$ and let f_n be the n th partial Fourier sum of the function f . Define the function space of trigonometric polynomials of degree at most n by*

$$\mathcal{G}_n = \text{span} \left\{ 1, \cos\left(\frac{2\pi k u}{T}\right), \sin\left(\frac{2\pi k u}{T}\right) : 1 \leq k \leq n \right\}$$

(i) f_n is the unique minimizer of the L^2 approximation error over the space \mathcal{G}_n , i.e.,

$$f_n = \underset{g \in \mathcal{G}_n}{\text{argmin}} \|f - g\|_{L^2}.$$

(ii) For all $n \in \mathbb{N} \setminus \{0\}$, the strict inequality

$$\|f - f_n\|_{L^2} < \|f - f_0\|_{L^2}$$

holds if and only if f is not equal to constant almost everywhere on $[0, T]$.

Proof. We first prove part (i). The Fourier coefficients of f on the interval $[0, T]$ are defined by

$$\begin{aligned}\alpha_0 &= \frac{1}{T} \int_0^T f(u) du, \\ \alpha_k &= \frac{2}{T} \int_0^T f(u) \cos\left(\frac{2\pi k u}{T}\right) du, \text{ for } k \geq 1, \\ \beta_k &= \frac{2}{T} \int_0^T f(u) \sin\left(\frac{2\pi k u}{T}\right) du, \text{ for } k \geq 1.\end{aligned}\tag{14}$$

Note that we have, for $j, k \geq 1$,

$$\int_0^T \cos\left(\frac{2\pi j u}{T}\right) \cos\left(\frac{2\pi k u}{T}\right) du = \frac{T}{2} \delta_{jk}, \quad \int_0^T \sin\left(\frac{2\pi j u}{T}\right) \sin\left(\frac{2\pi k u}{T}\right) du = \frac{T}{2} \delta_{jk}, \quad \int_0^T \cos\left(\frac{2\pi j u}{T}\right) \sin\left(\frac{2\pi k u}{T}\right) du = 0,\tag{15}$$

where δ_{jk} is the Kronecker delta and it is equal to 1 if $j = k$ and 0 otherwise.

Now let $g \in \mathcal{G}_n$ be an arbitrary trigonometric polynomial of the form

$$g(u) = a_0 + \sum_{k=1}^n \left[a_k \cos\left(\frac{2\pi k u}{T}\right) + b_k \sin\left(\frac{2\pi k u}{T}\right) \right].$$

Expanding the squared L^2 norm error $\|f - g\|_{L^2}^2$, we have that

$$\|f - g\|_{L^2}^2 = \|f\|_{L^2}^2 - 2\langle f, g \rangle_{L^2} + \|g\|_{L^2}^2.\tag{16}$$

For the inner product $\langle f, g \rangle_{L^2}$ in (16), we have from (14) that

$$\begin{aligned}\langle f, g \rangle_{L^2} &= \int_0^T f(u) \left[a_0 + \sum_{k=1}^n \left(a_k \cos\left(\frac{2\pi k u}{T}\right) + b_k \sin\left(\frac{2\pi k u}{T}\right) \right) \right] du \\ &= a_0 \int_0^T f(u) du + \sum_{k=1}^n \left[a_k \int_0^T f(u) \cos\left(\frac{2\pi k u}{T}\right) du + b_k \int_0^T f(u) \sin\left(\frac{2\pi k u}{T}\right) du \right] \\ &= T\alpha_0 a_0 + \frac{T}{2} \sum_{k=1}^n (\alpha_k a_k + \beta_k b_k).\end{aligned}\tag{17}$$

For the squared norm $\|g\|_{L^2}^2$ in (16), we have from (15) that

$$\begin{aligned}\|g\|_{L^2}^2 &= \int_0^T \left[a_0 + \sum_{k=1}^n \left(a_k \cos\left(\frac{2\pi k u}{T}\right) + b_k \sin\left(\frac{2\pi k u}{T}\right) \right) \right]^2 du. \\ &= a_0^2 \cdot T + \sum_{k=1}^n \left[a_k^2 \cdot \frac{T}{2} + b_k^2 \cdot \frac{T}{2} \right] = T a_0^2 + \frac{T}{2} \sum_{k=1}^n (a_k^2 + b_k^2)\end{aligned}\tag{18}$$

It then follows from (16), (17) and (18) that

$$\begin{aligned}\|f - g\|_{L^2}^2 &= \|f\|_{L^2}^2 - 2 \left[T\alpha_0 a_0 + \frac{T}{2} \sum_{k=1}^n (\alpha_k a_k + \beta_k b_k) \right] + T a_0^2 + \frac{T}{2} \sum_{k=1}^n (a_k^2 + b_k^2) \\ &= \|f\|_{L^2}^2 + T(a_0^2 - 2\alpha_0 a_0) + \frac{T}{2} \sum_{k=1}^n [(a_k^2 - 2\alpha_k a_k) + (b_k^2 - 2\beta_k b_k)] \\ &= \|f\|_{L^2}^2 - T\alpha_0^2 - \frac{T}{2} \sum_{k=1}^n (\alpha_k^2 + \beta_k^2) + T(\alpha_0 - a_0)^2 + \frac{T}{2} \sum_{k=1}^n [(\alpha_k - a_k)^2 + (\beta_k - b_k)^2].\end{aligned}\tag{19}$$

Recall that the n th partial Fourier sum is

$$f_n(u) = \alpha_0 + \sum_{k=1}^n \left[\alpha_k \cos\left(\frac{2\pi k u}{T}\right) + \beta_k \sin\left(\frac{2\pi k u}{T}\right) \right].\tag{20}$$

Replacing g in $\|f - g\|_{L^2}^2$ with f_n given in (20), we have that

$$\|f - f_n\|_{L^2}^2 = \|f\|_{L^2}^2 - T\alpha_0^2 - \frac{T}{2} \sum_{k=1}^n (\alpha_k^2 + \beta_k^2). \quad (21)$$

Substituting (21) back into (19), we obtain

$$\|f - g\|_{L^2}^2 = \|f - f_n\|_{L^2}^2 + T(\alpha_0 - a_0)^2 + \frac{T}{2} \sum_{k=1}^n [(\alpha_k - a_k)^2 + (\beta_k - b_k)^2]. \quad (22)$$

Since all terms on the right-hand side of (22) beyond $\|f - f_n\|_{L^2}^2$ are non-negative, it follows that $\|f - g\|_{L^2}^2 \geq \|f - f_n\|_{L^2}^2$ for all $g \in \mathcal{G}_n$. Moreover, equality holds if and only if $\alpha_0 = a_0$, $\alpha_k = a_k$ and $\beta_k = b_k$ for all $k \in \{1, \dots, n\}$. This establishes that f_n is the unique minimizer of the L^2 approximation error over \mathcal{G}_n , which completes the first part of the proof.

We next prove part (ii). In the first part of the proof, we have shown that

$$\|f - f_n\|_{L^2}^2 = \|f\|_{L^2}^2 - T\alpha_0^2 - \frac{T}{2} \sum_{k=1}^n (\alpha_k^2 + \beta_k^2).$$

In particular, for $n = 0$, this gives $\|f - f_0\|_{L^2}^2 = \|f\|_{L^2}^2 - Ta_0^2$. Taking the difference between $\|f - f_0\|_{L^2}^2$ and $\|f - f_n\|_{L^2}^2$, we obtain

$$\|f - f_0\|_{L^2}^2 - \|f - f_N\|_{L^2}^2 = \frac{T}{2} \sum_{k=1}^N (\alpha_k^2 + \beta_k^2). \quad (23)$$

Since each term at the right-hand side of equation (23) is non-negative, we have $\|f - f_N\|_{L^2} \leq \|f - f_0\|_{L^2}$ for all $N \geq 1$, with strict inequality if and only if at least one of $\alpha_1, \beta_1, \dots, \alpha_n, \beta_n$ is non-zero.

It then remains to show that at least one of $\alpha_1, \beta_1, \dots, \alpha_n, \beta_n$ is non-zero is equivalent to the statement that f is not equal to constant almost everywhere on $[0, T]$. We will prove the contrapositive statement. First recall that the constant functions on $[0, T]$ form the one-dimensional subspace

$$\text{span}\{1\} \subset L^2([0, T]).$$

Suppose that f is equal to a constant almost everywhere on $[0, T]$. Since $\cos(2\pi k u/T)$ and $\sin(2\pi k u/T)$ are orthogonal to constant functions in the space $L^2([0, T])$, $\alpha_k = \beta_k = 0$ for all $k \geq 1$. It then follows that $f(u) = \alpha_0$ almost everywhere. Conversely, suppose that for all $k \geq 1$, $\alpha_k = \beta_k = 0$. Then the Fourier series of f reduces to the constant term α_0 , and the partial Fourier sums satisfy that for all $n \in \mathbb{N}$,

$$f_n(u) = \alpha_0.$$

Since $f_n \rightarrow f \in L^2([0, T])$, it follows that $f = \alpha_0$ almost everywhere on $[0, T]$. Therefore, at least one of $\alpha_1, \beta_1, \dots, \alpha_n, \beta_n$ being nonzero is equivalent to f not being almost everywhere equal to a constant function on $[0, T]$. This completes the proof of part (ii) and hence the theorem. \square

D. Proof of Theorem 4.2

To prove Theorem 4.2, we proceed in three steps. First, we derive the DSQ gradient, as stated in Lemma D.1. Next, we establish the expectation and variance formulas for the DSQ and StableQAT schemes, respectively, which are given in Lemma D.3. Finally, we complete the proof of Theorem 4.2 by combining these results.

DSQ details. To address the non-differentiability of standard quantization, DSQ introduces a smooth asymptotic function $\phi(\cdot)$ that approximates each step of the uniform staircase quantizer. Specifically, the clipping range $[l, u]$ is uniformly partitioned into $2^b - 1$ intervals with width as $\Delta = \frac{u-l}{2^b-1}$ and the i -th quantization interval defined as

$$P_i = [l + i\Delta, l + (i + 1)\Delta), i \in \{0, \dots, 2^b - 2\}.$$

For an input $x \in P_i$, the smooth approximation is given by

$$\phi(x) = s \cdot \tanh(k(x - m_i)), \quad (24)$$

where $m_i = l + (i + \frac{1}{2})\Delta$ denotes the midpoint of i -th quantization interval P_i , and scaling factor $s = \frac{1}{\tanh((k\Delta)/2)}$ ensures continuity of $\phi(\cdot)$ across adjacent intervals. The parameter k controls the sharpness of the approximation, with larger values yielding a closer match to the hard staircase quantizer. To allow learnable control over the quantization sharpness, DSQ introduces a variable $\alpha \in (0, 1)$, which measures the approximation gap between soft and hard quantization and is defined as

$$\alpha = 1 - \tanh\left(\frac{1}{2}k\Delta\right). \quad (25)$$

Under this parameterization, the asymptotic function is fully determined by α and Δ with

$$s = \frac{1}{1 - \alpha}, \quad k = \frac{1}{\Delta} \ln\left(\frac{2 - \alpha}{\alpha}\right). \quad (26)$$

Combining (25) and (26) allows us to have the identity

$$\alpha = 1 - \tanh\left(\frac{1}{2} \ln\left(\frac{2 - \alpha}{\alpha}\right)\right). \quad (27)$$

Based on the asymptotic function $\phi(\cdot)$, the differentiable soft quantization (DSQ) function is defined as

$$Q_{\text{DSQ}}(x) = \begin{cases} l, & x < l, \\ u, & x > u, \\ l + \Delta\left(i + \frac{\phi(x) + 1}{2}\right), & x \in P_i. \end{cases} \quad (28)$$

Having established the DSQ formulation, we first derive the gradient of the DSQ function.

Lemma D.1 (DSQ Gradient). *Given the input $x \in P_i$, the gradient of the differentiable soft quantization function $Q_{\text{DSQ}}(x)$ defined in (28) is*

$$g_{\text{DSQ}}(x) = \frac{\partial Q_{\text{DSQ}}(x)}{\partial x} = \frac{\ln\left(\frac{2-\alpha}{\alpha}\right)}{2(1-\alpha)} \cdot \operatorname{sech}^2\left(\frac{\ln\left(\frac{2-\alpha}{\alpha}\right)}{\Delta}(x - m_i)\right) \quad (29)$$

Proof. Using the definition of DSQ function (See (28)) and the fact that $\frac{d}{du} \tanh(u) = \operatorname{sech}^2(u)$, we obtain that for all $x \in P_i$,

$$\frac{\partial Q_{\text{DSQ}}(x)}{\partial x} = \frac{\Delta}{2} \cdot s \cdot k \cdot \operatorname{sech}^2(k(x - m_i)).$$

Substituting $s = \frac{1}{1-\alpha}$ and $k = \frac{1}{\Delta} \ln\left(\frac{2-\alpha}{\alpha}\right)$ provided in (26) yields the result (29), which completes the proof. \square

We first present several existing integral results, which will be used to derive the expectation and variance of the StableQAT and DSQ schemes, respectively.

Lemma D.2. *The following integral identities hold:*

(i) *If $c^2 < 1$, then*

$$\int_{-\frac{\pi}{2}}^{\frac{\pi}{2}} \frac{1}{1 + c \cos x} dx = \frac{4}{\sqrt{1 - c^2}} \arctan\left(\sqrt{\frac{1 - c}{1 + c}}\right).$$

(ii) *If $c^2 < 1$, then*

$$\int_{-\frac{\pi}{2}}^{\frac{\pi}{2}} \frac{1}{(1 + c \cos x)^2} dx = \frac{4}{(1 - c^2)^{3/2}} \arctan\left(\sqrt{\frac{1 - c}{1 + c}}\right) - \frac{2c}{1 - c^2}.$$

(iii) *Given any $c > 0$,*

$$\int_{-c}^c \operatorname{sech}^4(x) dx = 2 \left(\tanh(c) - \frac{\tanh^3(c)}{3} \right).$$

Proof. (i) Using the result from (Gradshteyn & Ryzhik, 2007) and the fact that $c^2 < 1$, we have that

$$\int_{-\pi/2}^{\pi/2} \frac{1}{1+c \cos x} dx = \frac{2}{\sqrt{1-c^2}} \arctan \left(\frac{(1-c) \tan \left(\frac{x}{2} \right)}{\sqrt{1-c^2}} \right) \Big|_{-\pi/2}^{\pi/2} = \frac{4}{\sqrt{1-c^2}} \arctan \left(\sqrt{\frac{1-c}{1+c}} \right),$$

as claimed.

(ii) It follows from (Gradshteyn & Ryzhik, 2007) and the fact that $c^2 < 1$ that

$$\begin{aligned} \int_{-\pi/2}^{\pi/2} \frac{1}{(1+c \cos x)^2} dx &= -\frac{1}{1-c^2} \left\{ \frac{c \sin(x)}{1+c \cos(x)} - \frac{2}{\sqrt{1-c^2}} \arctan \left(\frac{(1-c) \tan \left(\frac{x}{2} \right)}{\sqrt{1-c^2}} \right) \right\} \Big|_{-\pi/2}^{\pi/2} \\ &= \frac{4}{(1-c^2)^{3/2}} \arctan \left(\sqrt{\frac{1-c}{1+c}} \right) - \frac{2c}{1-c^2}, \end{aligned}$$

as claimed.

(iii) Let $u = \tanh(x)$ and this gives $du = \operatorname{sech}^2(x) dx$. It then follows from the fact that $\operatorname{sech}^4(x) = \operatorname{sech}^2(x) \cdot (1 - \tanh^2(x))$ that

$$\int_{-c}^c \operatorname{sech}^4(x) dx = \int_{\tanh(-c)}^{\tanh(c)} (1-u^2) du = \left[u - \frac{u^3}{3} \right]_{\tanh(-c)}^{\tanh(c)} = 2 \left(\tanh(c) - \frac{\tanh^3(c)}{3} \right),$$

as claimed. \square

With these integral identities, we can now derive closed-form expressions for the statistical properties of each gradient estimator. The following lemma provides the expectation and variance under uniform sampling.

Lemma D.3 (Expectation and variance). *The expectation and variance of the gradient estimators under DSQ and StableQAT schemes are given as follows.*

1. (DSQ)

$$\mathbb{E}_{\xi \sim U(l,u)}[g_{\text{DSQ}}(x; \alpha)] = 1, \operatorname{Var}_{\xi \sim U(l,u)}[g_{\text{DSQ}}(x; \alpha)] = \frac{\ln\left(\frac{2-\alpha}{\alpha}\right)(3 - (1-\alpha)^2)}{6(1-\alpha)} - 1.$$

2. (StableQAT)

Let $c = \sqrt{2}\pi A$ with $A \in (0, \frac{1}{\sqrt{2}\pi})$. Then,

$$\begin{aligned} \mathbb{E}_{\xi \sim U(l,u)}[g_{\text{StableQAT}}(x; A)] &= \frac{8}{\pi\sqrt{1-c^2}} \arctan \left(\sqrt{\frac{1-c}{1+c}} \right) - 1, \\ \operatorname{Var}_{\xi \sim U(l,u)}[g_{\text{StableQAT}}(x; A)] &= \frac{16}{\pi(1-c^2)^{3/2}} \arctan \left(\sqrt{\frac{1-c}{1+c}} \right) - \frac{8c}{\pi(1-c^2)} + 1 - \left(\frac{8}{\pi\sqrt{1-c^2}} \arctan \left(\sqrt{\frac{1-c}{1+c}} \right) - 1 \right)^2. \end{aligned}$$

Proof. For notation brevity, we use $\mathbb{E}[\cdot]$ to denote $\mathbb{E}_{\xi \sim U(l,u)}[\cdot]$ and $\operatorname{Var}[\cdot]$ to denote $\operatorname{Var}_{\xi \sim U(l,u)}[\cdot]$. Let $\beta = \ln\left(\frac{2-\alpha}{\alpha}\right)$.

DSQ Expectation. We have from Lemma D.1, change of variable trick, the fact that range $[l, u]$ has $2^b - 1$ interval with length Δ , $\frac{d}{dx} \tanh(x) = \operatorname{sech}^2(x)$, and (27) that

$$\begin{aligned}
 \mathbb{E}[g_{\text{DSQ}}(\xi; \alpha)] &= \sum_{i=0}^{2^b-2} \int_{m_i - \frac{\Delta}{2}}^{m_i + \frac{\Delta}{2}} \frac{\beta}{2(1-\alpha)} \cdot \operatorname{sech}^2\left(\frac{\beta}{\Delta}(\xi - m_i)\right) \cdot \frac{1}{u-l} d\xi \\
 &= \sum_{i=0}^{2^b-2} \int_{-\frac{\Delta}{2}}^{\frac{\Delta}{2}} \frac{\beta}{2(1-\alpha)} \cdot \operatorname{sech}^2\left(\frac{\beta}{\Delta}\xi\right) \cdot \frac{1}{u-l} d\xi \\
 &= \frac{2^b - 1}{u-l} \int_{-\frac{\Delta}{2}}^{\frac{\Delta}{2}} \frac{\beta}{2(1-\alpha)} \cdot \operatorname{sech}^2\left(\frac{\beta}{\Delta}\xi\right) d\xi \\
 &= \frac{1}{\Delta} \int_{-\frac{\Delta}{2}}^{\frac{\Delta}{2}} \frac{\beta}{2(1-\alpha)} \cdot \operatorname{sech}^2\left(\frac{\beta}{\Delta}\xi\right) d\xi \\
 &= \frac{1}{\Delta} \cdot \frac{\beta}{2(1-\alpha)} \cdot \frac{\Delta}{\beta} \cdot \tanh\left(\frac{\beta}{\Delta}\xi\right) \Big|_{-\frac{\Delta}{2}}^{\frac{\Delta}{2}} \\
 &= \frac{1}{1-\alpha} \tanh\left(\frac{\beta}{2}\right) = \frac{1}{1-\alpha} \tanh\left(\frac{1}{2} \ln\left(\frac{2-\alpha}{\alpha}\right)\right) = 1.
 \end{aligned} \tag{30}$$

DSQ Variance. To compute DSQ variance, one first need to compute the second order moment of random variable $g_{\text{DSQ}}(\xi; \alpha)$. We have from Lemma D.1, change of variable trick, the fact that range $[l, u]$ has $2^b - 1$ interval with length Δ , Lemma D.2(iii), and (27) that

$$\begin{aligned}
 \mathbb{E}[g_{\text{DSQ}}^2(\xi; \alpha)] &= \sum_{i=0}^{2^b-2} \int_{m_i - \frac{\Delta}{2}}^{m_i + \frac{\Delta}{2}} \left(\frac{\ln\left(\frac{2-\alpha}{\alpha}\right)}{2(1-\alpha)}\right)^2 \cdot \operatorname{sech}^4\left(\frac{\ln\left(\frac{2-\alpha}{\alpha}\right)}{\Delta}(\xi - m_i)\right) \cdot \frac{1}{u-l} d\xi \\
 &= \sum_{i=0}^{2^b-2} \int_{-\frac{\Delta}{2}}^{\frac{\Delta}{2}} \left(\frac{\beta}{2(1-\alpha)}\right)^2 \operatorname{sech}^4\left(\frac{\beta}{\Delta}\xi\right) d\xi \\
 &= \frac{1}{\Delta} \int_{-\frac{\beta}{2}}^{\frac{\beta}{2}} \left(\frac{\beta}{2(1-\alpha)}\right)^2 \cdot \frac{\Delta}{\beta} \cdot \operatorname{sech}^4(\xi) d\xi \\
 &= \frac{\beta}{4(1-\alpha)^2} \int_{-\frac{\beta}{2}}^{\frac{\beta}{2}} \operatorname{sech}^4(\xi) d\xi \\
 &= \frac{\beta}{4(1-\alpha)^2} \left(2 \tanh\left(\frac{\beta}{2}\right) - \frac{2}{3} \tanh^3\left(\frac{\beta}{2}\right)\right) \\
 &= \frac{\beta}{4(1-\alpha)^2} \left(2(1-\alpha) - \frac{2}{3}(1-\alpha)^3\right) = \frac{\ln\left(\frac{2-\alpha}{\alpha}\right) \cdot (3 - (1-\alpha)^2)}{6(1-\alpha)}.
 \end{aligned} \tag{31}$$

It then follows from the definition of variance, (30) and (31) that

$$\operatorname{Var}[g_{\text{DSQ}}(\xi; \alpha)] = \mathbb{E}[g_{\text{DSQ}}^2(\xi; \alpha)] - (\mathbb{E}[g_{\text{DSQ}}(\xi; \alpha)])^2 = \frac{\ln\left(\frac{2-\alpha}{\alpha}\right) \cdot (3 - (1-\alpha)^2)}{6(1-\alpha)} - 1.$$

For $N = 1$, the StableQAT gradient is given as for all $\xi \in [l, u]$,

$$g_{\text{StableQAT}}(\xi) = \frac{1 - \sqrt{2}\pi A \cos\left(\pi\left(\frac{\xi}{\Delta} + \left\lfloor \frac{\xi}{\Delta} \right\rfloor\right)\right)}{1 + \sqrt{2}\pi A \cos\left(\pi\left(\frac{\xi}{\Delta} + \left\lfloor \frac{\xi}{\Delta} \right\rfloor\right)\right)} = \frac{1 - c \cdot \cos\left(\pi\left(\frac{\xi}{\Delta} - \left\lfloor \frac{\xi}{\Delta} \right\rfloor\right)\right)}{1 + c \cdot \cos\left(\pi\left(\frac{\xi}{\Delta} - \left\lfloor \frac{\xi}{\Delta} \right\rfloor\right)\right)}. \tag{32}$$

StableQAT Expectation. Using (32), the change of variable trick ($\theta = \frac{x}{\Delta} - \lfloor \frac{x}{\Delta} \rfloor$), the fact that range $[l, u]$ has $2^b - 1$ interval with length Δ , and Lemma D.2(i) that

$$\begin{aligned}
 \mathbb{E}[g_{\text{StableQAT}}(\xi; A)] &= \int_l^u g_{\text{StableQAT}}(\xi) \cdot \frac{1}{u-l} d\xi \\
 &= \sum_{i=0}^{2^b-3} \int_{m_i}^{m_{i+1}} g_{\text{StableQAT}}(\xi) \cdot \frac{1}{u-l} d\xi + \int_l^{l+\frac{\Delta}{2}} g_{\text{StableQAT}}(\xi) \cdot \frac{1}{u-l} d\xi + \int_{u-\frac{\Delta}{2}}^u g_{\text{StableQAT}}(\xi) \cdot \frac{1}{u-l} d\xi \\
 &= \sum_{i=0}^{2^b-3} \int_{-\frac{\pi}{2}}^{\frac{\pi}{2}} \frac{1-c \cdot \cos(\theta)}{1+c \cdot \cos(\theta)} \cdot \frac{\Delta}{\pi(u-l)} d\theta + \int_0^{\frac{\pi}{2}} \frac{1-c \cdot \cos(\theta)}{1+c \cdot \cos(\theta)} \cdot \frac{\Delta}{\pi(u-l)} d\theta + \int_{-\frac{\pi}{2}}^0 \frac{1-c \cdot \cos(\theta)}{1+c \cdot \cos(\theta)} \cdot \frac{\Delta}{\pi(u-l)} d\theta \\
 &= \frac{(2^b-1)\Delta}{u-l} \cdot \frac{1}{\pi} \int_{-\frac{\pi}{2}}^{\frac{\pi}{2}} \frac{1-c \cdot \cos(\theta)}{1+c \cdot \cos(\theta)} d\theta \\
 &= \frac{1}{\pi} \int_{-\frac{\pi}{2}}^{\frac{\pi}{2}} \frac{1-c \cdot \cos(\theta)}{1+c \cdot \cos(\theta)} d\theta \\
 &= \frac{1}{\pi} \int_{-\frac{\pi}{2}}^{\frac{\pi}{2}} \left(\frac{2}{1+c \cos \theta} - 1 \right) d\theta \\
 &= \frac{8}{\pi \sqrt{1-c^2}} \arctan \left(\sqrt{\frac{1-c}{1+c}} \right) - 1.
 \end{aligned} \tag{33}$$

StableQAT Variance. Using the change of variable trick ($\theta = \frac{\xi}{\Delta} - \lfloor \frac{\xi}{\Delta} \rfloor$), the fact that range $[l, u]$ has $2^b - 1$ interval with length Δ , and Lemma D.2(i)-(ii) that

$$\begin{aligned}
 \mathbb{E}[g_{\text{StableQAT}}^2(\xi; A)] &= \int_l^u g_{\text{StableQAT}}^2(\xi) \cdot \frac{1}{u-l} d\xi \\
 &= \sum_{i=0}^{2^b-3} \int_{m_i}^{m_{i+1}} g_{\text{StableQAT}}^2(\xi) \cdot \frac{1}{u-l} d\xi + \int_l^{l+\frac{\Delta}{2}} g_{\text{StableQAT}}^2(\xi) \cdot \frac{1}{u-l} d\xi + \int_{u-\frac{\Delta}{2}}^u g_{\text{StableQAT}}^2(\xi) \cdot \frac{1}{u-l} d\xi \\
 &= \sum_{i=0}^{2^b-3} \int_{-\frac{\pi}{2}}^{\frac{\pi}{2}} \left(\frac{1-c \cdot \cos(\theta)}{1+c \cdot \cos(\theta)} \right)^2 \cdot \frac{\Delta}{\pi(u-l)} d\theta + \int_0^{\frac{\pi}{2}} \left(\frac{1-c \cdot \cos(\theta)}{1+c \cdot \cos(\theta)} \right)^2 \cdot \frac{\Delta}{\pi(u-l)} d\theta + \int_{-\frac{\pi}{2}}^0 \left(\frac{1-c \cdot \cos(\theta)}{1+c \cdot \cos(\theta)} \right)^2 \cdot \frac{\Delta}{\pi(u-l)} d\theta \\
 &= \frac{(2^b-1)\Delta}{\pi(u-l)} \int_{-\frac{\pi}{2}}^{\frac{\pi}{2}} \left(\frac{1-c \cdot \cos(\theta)}{1+c \cdot \cos(\theta)} \right)^2 d\theta \\
 &= \frac{1}{\pi} \int_{-\frac{\pi}{2}}^{\frac{\pi}{2}} \left(\frac{1-c \cdot \cos(\theta)}{1+c \cdot \cos(\theta)} \right)^2 d\theta \\
 &= \frac{1}{\pi} \int_{-\frac{\pi}{2}}^{\frac{\pi}{2}} \frac{4}{(1+c \cdot \cos \theta)^2} - \frac{4}{1+c \cdot \cos \theta} + 1 d\theta \\
 &= \frac{16}{\pi(1-c^2)^{3/2}} \arctan \left(\sqrt{\frac{1-c}{1+c}} \right) - \frac{8c}{\pi(1-c^2)} + 1 - \frac{16}{\pi \sqrt{1-c^2}} \arctan \left(\sqrt{\frac{1-c}{1+c}} \right).
 \end{aligned} \tag{34}$$

It then follows from (33) and (34) that

$$\begin{aligned}
 \text{Var}[g_{\text{StableQAT}}(\xi; A)] &= \mathbb{E}[g_{\text{StableQAT}}^2(\xi; A)] - (\mathbb{E}[g_{\text{StableQAT}}(\xi; A)])^2 \\
 &= \frac{16c^2}{\pi(1-c^2)^{3/2}} \arctan \left(\sqrt{\frac{1-c}{1+c}} \right) - \frac{8c}{\pi(1-c^2)} + 1 - \left(\frac{8}{\pi \sqrt{1-c^2}} \arctan \left(\sqrt{\frac{1-c}{1+c}} \right) - 1 \right)^2.
 \end{aligned}$$

□

Now, we are ready to prove Theorem 4.2.

Proof of Theorem 4.2. We establish each limit separately, drawing upon the closed-form expressions derived in Lemma D.3. Throughout, we denote $c = \sqrt{2\pi}A$ and note that as $A \rightarrow \left(\frac{1}{\sqrt{2\pi}}\right)^-$, we have $c \rightarrow 1^-$.

DSQ expectation limit. From Lemma D.3, the expected value of the DSQ gradient satisfies $\mathbb{E}_{\xi \sim U(l,u)}[g_{\text{DSQ}}(\xi)] = 1$ for all $\alpha \in (0, 1)$. Since this identity is independent of α , it follows that

$$\lim_{\alpha \rightarrow 0^+} \mathbb{E}[g_{\text{DSQ}}(\xi; \alpha)] = 1.$$

StableQAT expectation limit. From Lemma D.3, the expectation of the StableQAT gradient is given by

$$\mathbb{E}_{\xi \sim U(l,u)}[g_{\text{StableQAT}}(\xi; A)] = \frac{8}{\pi\sqrt{1-c^2}} \arctan\left(\sqrt{\frac{1-c}{1+c}}\right) - 1.$$

It then follows from the fact that $\lim_{x \rightarrow 0} \frac{\arctan(x)}{x} = 1$ that

$$\begin{aligned} \lim_{A \rightarrow \left(\frac{1}{\sqrt{2\pi}}\right)^-} \mathbb{E}[g_{\text{StableQAT}}(x)] &= \lim_{c \rightarrow 1^-} \frac{8}{\pi\sqrt{1-c^2}} \arctan\left(\sqrt{\frac{1-c}{1+c}}\right) - 1 \\ &= \lim_{c \rightarrow 1^-} \frac{\arctan\left(\sqrt{\frac{1-c}{1+c}}\right)}{\left(\sqrt{\frac{1-c}{1+c}}\right)} \cdot \frac{8}{\pi\sqrt{1-c^2}} - 1 = \frac{4}{\pi} - 1. \end{aligned} \tag{35}$$

DSQ variance limit. From Lemma D.3, the variance of the DSQ gradient is given by

$$\text{Var}_{\xi \sim U(l,u)}[g_{\text{DSQ}}(\xi; \alpha)] = \frac{\ln\left(\frac{2-\alpha}{\alpha}\right)(3 - (1-\alpha)^2)}{6(1-\alpha)} - 1. \tag{36}$$

We first analyze the asymptotic behavior of each factor as $\alpha \rightarrow 0^+$ as follows.

$$\lim_{\alpha \rightarrow 0^+} \ln\left(\frac{2-\alpha}{\alpha}\right) = +\infty, \lim_{\alpha \rightarrow 0^+} (1-\alpha) = 1, \lim_{\alpha \rightarrow 0^+} (3 - (1-\alpha)^2) = 2. \tag{37}$$

Combining (36) and (37) allows us to have that

$$\lim_{\alpha \rightarrow 0^+} \text{Var}[g_{\text{DSQ}}(\xi; \alpha)] = \lim_{\alpha \rightarrow 0^+} \frac{\ln\left(\frac{2-\alpha}{\alpha}\right)(3 - (1-\alpha)^2)}{6(1-\alpha)} - 1 = +\infty.$$

StableQAT variance limit. From Lemma D.3, the variance of the StableQAT gradient is given by

$$\text{Var}_{\xi \sim U(l,u)}[g_{\text{StableQAT}}(\xi; A)] = \underbrace{\frac{16c^2}{\pi(1-c^2)^{3/2}} \arctan\left(\sqrt{\frac{1-c}{1+c}}\right) - \frac{8c}{\pi(1-c^2)} + 1}_{T_1(c)} - \underbrace{\left(\frac{8}{\pi\sqrt{1-c^2}} \arctan\left(\sqrt{\frac{1-c}{1+c}}\right) - 1\right)^2}_{T_2(c)}.$$

We note that $\lim_{c \rightarrow 1^-} T_2(c)$ has been derived in (35). To this end, it remains to compute $\lim_{c \rightarrow 1^-} T_1(c)$. Let $u^2 = \frac{1-c}{1+c}$ and this implies that

$$c = \frac{1-u^2}{1+u^2} \text{ and } 1-c^2 = \frac{4u^2}{(1+u^2)^2}. \tag{38}$$

Then, using (38) and Taylor series expansion of function $\arctan(x)$ at $x = 0$, we have that

$$\begin{aligned}
 \lim_{c \rightarrow 1^-} T_1(c) &= \lim_{u \rightarrow 0^+} \frac{16(1-u^2)^2}{\pi 8u^3} \arctan(u) - \frac{8 \left(\frac{1-u^2}{1+u^2} \right)}{\pi \left(\frac{4u^2}{(1+u^2)^2} \right)} \\
 &= \lim_{u \rightarrow 0^+} \frac{16(1-u^2)^2(1+u^2)}{\pi 8u^3} \left(u - \frac{u^3}{3} + O(u^5) \right) - \frac{8(1-u^2)(1+u^2)}{4\pi u^2} \\
 &= \lim_{u \rightarrow 0^+} \frac{16(1-u^2)^2(1+u^2)u}{24\pi} - \frac{8(1-u^2)(1+u^2)}{4\pi u^2} \\
 &= \lim_{u \rightarrow 0^+} \frac{2(1-u^2-u^4+u^6)}{3\pi} - \frac{2(1-2u^2+u^4)}{\pi u^2} \\
 &= \lim_{u \rightarrow 0^+} \left(-\frac{8}{3\pi} + O(u^2) \right) = -\frac{8}{3\pi}.
 \end{aligned} \tag{39}$$

Combining (35) and (39) allows us to have that

$$\lim_{A \rightarrow \left(\frac{1}{\sqrt{2}\pi}\right)^-} \text{Var}_{\xi \sim U(l, u)} [g_{\text{StableQAT}}(\xi; A)] = \lim_{c \rightarrow 1^-} T_1(c) + 1 - T_2(c) = \frac{16}{3\pi} - \frac{16}{\pi^2}.$$

□